ChemPubSoc Europe

DOI: 10.1002/cssc.201901850

CHEMSUSCHEM Communications

Wet-Chemical Tuning of $Li_{3-x}PS_4$ ($0 \le x \le 0.3$) Enabled by Dual Solvents for All-Solid-State Lithium-Ion Batteries

Dae Yang Oh[+],[a] A. Reum Ha[+],[a] Ji Eun Lee[+],[a] Sung Hoo Jung,[a] Goojin Jeong,[b] Woosuk Cho,[b] Kyung Su Kim,[b] and Yoon Seok Jung*[a]

All-solid-state lithium-ion batteries (ASLBs) employing sulfide solid electrolytes are attractive next-generation rechargeable batteries that could offer improved safety and energy density. Recently, wet syntheses or processes for sulfide solid electrolyte materials have opened opportunities to explore new materials and practical fabrication methods for ASLBs. A new wet-chemical route for the synthesis of Li-deficient $Li_{3-x}PS_4$ ($0 \le x \le 0.3$) has been developed, which is enabled by dual solvents. Owing to its miscibility with tetrahydrofuran and ability to dissolve elemental sulfur, *o*-xylene as a cosolvent facilitates the wet-chemical synthesis of $Li_{3-x}PS_4$. $Li_{3-x}PS_4$ ($0 \le x \le 0.15$) derived by using dual solvents shows Li^+ conductivity of approximately 0.2 mS cm^{-1} at 30 °C, in contrast to 0.034 mS cm^{-1} for a sample obtained by using a conventional single solvent (tetrahydrofuran, $x = 0.15$). The evolution of the structure for $Li_{3-x}PS_4$ is also investigated by complementary analysis using X-ray diffraction, Raman, and X-ray photoelectron spectroscopy measurements. $LiCoO_2$/Li–In ASLBs employing $Li_{2.85}PS_4$ obtained by using dual solvents exhibit a reversible capacity of 130 mA h g^{-1} with good cycle retention at 30 °C, outperforming cells with $Li_{2.85}PS_4$ obtained by using a conventional single solvent.

Owing to the fast-growing demand for better safety and higher energy density of lithium-ion batteries, all-solid-state lithium-ion batteries (ASLBs) that replace flammable organic liquid electrolytes with inorganic solid electrolytes (SEs) have emerged as promising candidates for next-generation rechargeable batteries.[1] Consideration of various performance characteristics for SEs suggests that sulfide materials are highly competitive in the development of all-solid-state batteries on a large scale.[1e,2] Despite their drawback in terms of (electro)chemical stability, sulfide SE materials not only show high ionic conductivities in the range 0.1–21 mS cm^{-1} at room temperature with single-ion conducting properties but also show superb formability owing to excellent ductility (Young's modulus ≈ 20 GPa).[1e,3] In this regard, most room-temperature-operable state-of-the-art all-solid-state batteries have employed sulfide SEs.[1e,2b,4]

To date, several important classes of sulfide Li^+ or Na^+ solid ionic conductors have been developed, including glass-ceramic $x Li_2S$-$(100-x)P_2S_5$ ($50 \le x \le 80$),[5] argyrodite Li_6PS_5X (X = Cl, Br, I),[6] $Li_{10}GeP_2S_{12}$ family ($Li_{10}MP_2S_{12}$, M = Si, Ge, Sn),[4c,7] cubic Na_3PS_4,[8] Na_3SbS_4,[9] and $Na_{4-x}Sn_{1-x}M_xS_4$ (M = P, Sb).[10] Notably, the structure and (electro)chemical characteristics of the corresponding all-solid-state batteries are strongly associated with the configuration of the polyhedral anions (e.g., PS_4^{3-}, $P_2S_7^{4-}$, $P_2S_6^{4-}$, MS^{4-}).[5b,11] This opens a research avenue for fine-tuning of polyhedra and concomitant structural evolution towards development of new materials or enhancement of (electro)chemical performance. Compared with conventional β-Li_3PS_4 (0.1–1 mS cm^{-1}), the introduction of excess Li in Li_3PS_4 led to the identification of $Li_{9.6}P_3S_{12}$, which is isostructural with $Li_{10}GeP_2S_{12}$ (1.2 mS cm^{-1}).[4c] Also, decreasing the sulfur content to $Li_3PS_{3.83}$ increased the Li^+ conductivity significantly up to approximately 1 mS cm^{-1}.[12] For the preparation of these finely tuned $Li_{3+x}PS_{4-y}$ compounds, conventional synthetic protocols based on mechanochemical methods or solid-state reactions at high temperature were employed.

Recently, wet-chemical routes for sulfide SE materials, that is, liquid-phase syntheses and solution processes, have been developed.[1e] In typical liquid-phase syntheses, SE precursors (e.g., Li_2S and P_2S_5) react, aided by organic solvents such as tetrahydrofuran (THF) and acetonitrile, forming a suspension of intermediate products dispersed in the solvent.[13] In contrast, in the solution process, SE materials [e.g., Li_6PS_5X,[4e,14] (LiI-)Li_4SnS_4,[15] and (NaI-)Na_3SbS_4][1e,9] are fully dissolved in solvents (e.g., ethanol, methanol, or water), forming a homogeneous solution. In both routes, the final SE products are acquired by removing the solvents and subsequent heat treatment.

Since Liang and co-workers synthesized nanoporous β-Li_3PS_4 (0.16 mS cm^{-1}) by liquid-phase synthesis, which is otherwise unobtainable by conventional synthetic methods (γ-Li_3PS_4, $> 10^{-6}$ S cm^{-1}),[13] extensive efforts in liquid-phase synthesis and solution process have led to the identification and development of new materials, such as $Li_7P_2S_8I$ (0.6 mS cm^{-1}),[16] 0.4 LiI·0.6 Li_4SnS_4 (0.4 mS cm^{-1}),[15a] and argyrodite high-temperature phase Li_7PS_6 (0.1 mS cm^{-1}).[17] Furthermore, the wet-chemical routes provide new potentially advantageous features of mass production and morphology/size control,[1e,18] and new opportunities for the fabrication of all-solid-state bat-

[a] Dr. D. Y. Oh,[+] A. R. Ha,[+] J. E. Lee,[+] Dr. S. H. Jung, Prof. Y. S. Jung
Department of Energy Engineering
Hanyang University, Seoul 04763 (South Korea)
E-mail: yoonsjung@hanyang.ac.kr

[b] Dr. G. Jeong, Dr. W. Cho, Dr. K. S. Kim
Advanced Batteries Research Center
Korea Electronics Technology Institute, Seongnam 13509 (South Korea)

[+] These authors contributed equally to this work.

Supporting Information and the ORCID identification number(s) for the author(s) of this article can be found under: https://doi.org/10.1002/cssc.201901850.

teries, such as SE coating on active materials,[15] SE-infiltrated electrodes,[4e,19] and wet-tailored electrodes.[18a]

More recently, elaborate liquid-phase syntheses of sulfide SEs have been reported. High-purity β-Li_3PS_4 (0.13 mS cm^{-1}) was prepared by adding $LiSC_2H_5$ as a nucleophilic agent during the liquid-phase synthesis because the THF-soluble intermediate species of P_2S_5-$LiSC_2H_5$ stimulates the reactivity.[20] Adding excess sulfur for the liquid-phase synthesis of Li_3PS_4 allowed the conversion of the suspension into a homogeneous solution although the as-obtained SE materials showed poor conductivities of $< 10^{-5}$ S cm^{-1}.[20,21] Argyrodites Li_6PS_5X and high-temperature phase Li_7PS_6 were successfully synthesized from homogeneous solutions acquired from their precursors by using dual solvents (THF (or ethyl propionate or acetonitrile) and ethanol).[17,22] A recent investigation on the synthesis of $Li_7P_3S_{11}$ by using acetonitrile pointed out the importance of soluble species Li_2S-P_2S_5.[23] Although a full understanding of the underlying chemistry has not yet been achieved, the key to the aforementioned research might be related to the solubility of the SE precursors in the solvents.

Based on the aforementioned research background and inspiration, herein, we report the development of wet-chemically tuned $Li_{3-x}PS_4$ ($0 \le x \le 0.3$) for ASLBs, enabled by dual solvents. The use of *o*-xylene, which dissolves elemental sulfur, renders a THF-based liquid-phase synthesis of Li-deficient $Li_{3-x}PS_4$ with higher purity and narrower particle size distribution than conventional synthesis by using a single solvent (THF).

For the synthesis of Li-deficient $Li_{3-x}PS_4$, addition of elemental sulfur is required (see the Supporting Information, Table S1). For promoting a liquid-phase reaction involving elemental sulfur, solvents that can dissolve elemental sulfur and are miscible with THF are needed. In this regard, *o*-xylene was selected with the additional desirable physical properties of suitable vapor pressure (7 mmHg at 20 °C) and boiling point (144 °C). Figure 1a illustrates a schematic diagram for the liquid-phase synthesis of $Li_{3-x}PS_4$ ($0 \le x \le 0.3$) by using the dual solvents THF and *o*-xylene. Final white powders were obtained by stirring the reactant solution at 30 °C, followed by drying under vacuum and subsequent heat treatment at 150 °C (the detailed experimental procedure is shown in the Supporting Information). Morphology and particle size distribution were measured by field-emission scanning electron microscopy (FESEM) and a particle size analyzer. Hereafter, $Li_{3-x}PS_4$ ($0 \le x \le 0.3$) prepared by using specific solvents (THF or THF/*o*-xylene) is referred to as "LPS-*x*-solvent". First of all, a control experiment confirmed that $Li_{3.00}PS_4$ obtained by using dual solvents (LPS-0.00-THF/*o*-xylene) is not different from that obtained by using the conventional single solvent (LPS-0.00-THF) from the viewpoint of morphology and crystal structure (Figure S1) as well as a Li^+ conductivity of 0.2 mS cm^{-1} (Figure 2b). In contrast, the use of dual solvents resulted in distinct differences for the case of Li-deficient composition (LPS-0.15). In Figure 1b,c, whereas LPS-0.15-THF powders show segregated and irregular shapes, more regular rod-like shapes are observed for LPS-0.15-THF/*o*-xylene,

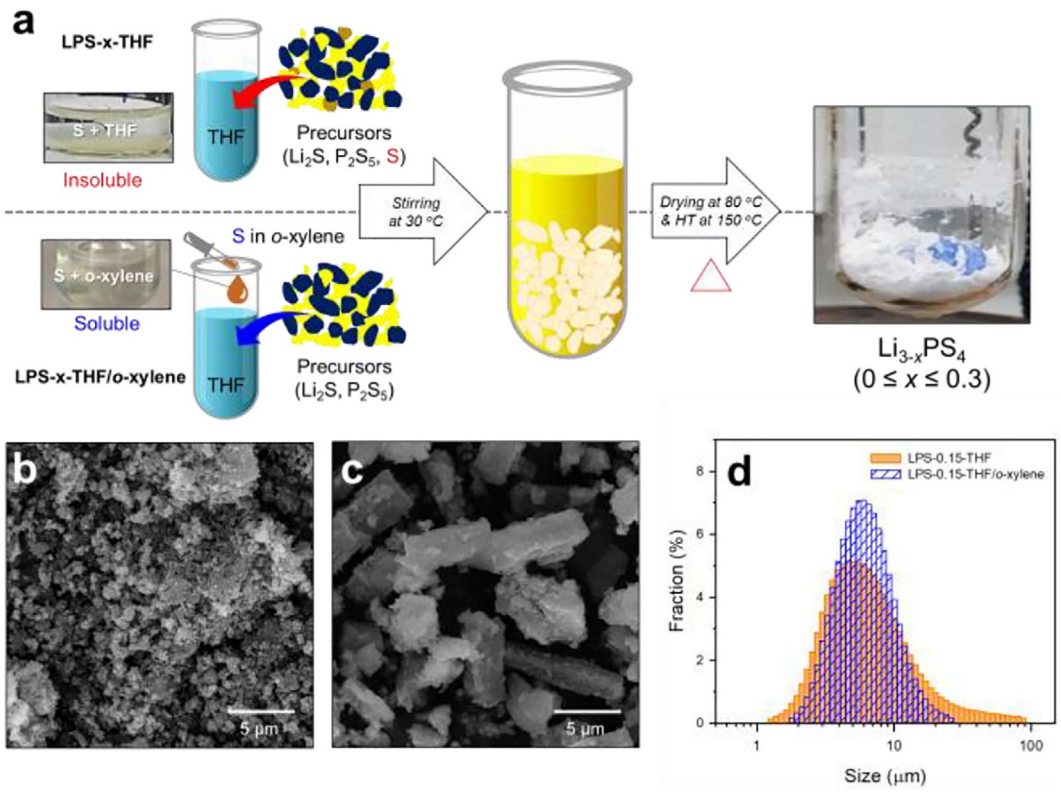

Figure 1. (a) Schematic diagram illustrating liquid-phase synthetic routes for Li-deficient $Li_{3-x}PS_4$ (LPS-*x*) using single solvent (THF) or dual solvents (THF/*o*-xylene). Photographs of sulfur in THF or *o*-xylene and $Li_{3-x}PS_4$ powders obtained by the use of dual solvents are shown. FESEM images of (b) LPS-0.15-THF and (c) LPS-0.15-THF/*o*-xylene. (d) Particle size distribution of the LPS-0.15-THF and LPS-0.15-THF/*o*-xylene.

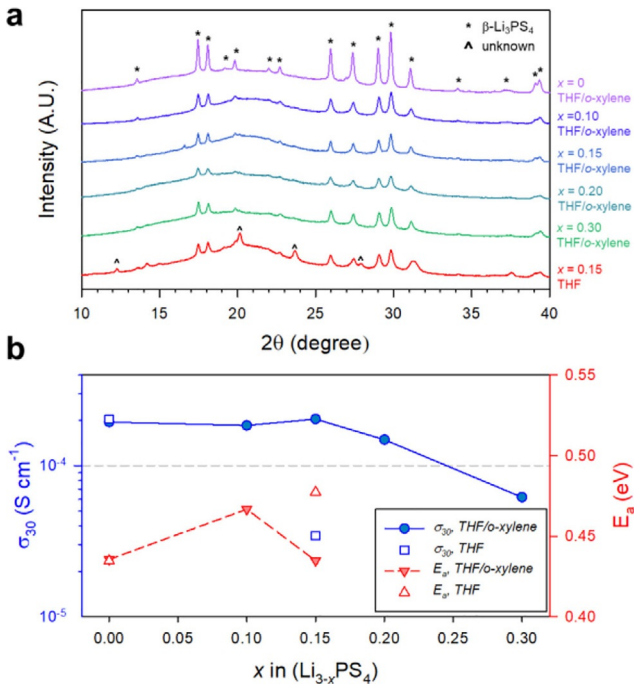

Figure 2. (a) XRD patterns and (b) Li^+ conductivities at 30 °C and the corresponding activation energies for the wet-chemically tuned $Li_{3-x}PS_4$ derived by using dual solvents of THF and *o*-xylene (LPS-*x*-THF/*o*-xylene) with varied *x*.

which is similar to the shape of LPS-0.00 (Figure S1). This observation is also consistent with the results of particle size analysis. Although the mean diameters (D_{50}) for LPS-0.15-THF and LPS-0.15-THF/*o*-xylene were almost identical, approximately 5.7 μm, LPS-1.5-THF/*o*-xylene showed much narrower particle size distribution, compared with that of its THF counterpart (Figure 1 d). The narrow particle size distribution of LPS-*x*-THF/*o*-xylene could be an advantageous feature for the application to all-solid-state batteries, in comparison with SEs prepared by conventional methods such as solid-state synthesis.[18] For example, performance of all-solid-state electrodes could be optimized by the use of two different SEs: one with insufficient conductivity but small particle size and another with large particle size but high conductivity. The former would help to facilitate the formation of intimate contacts with active materials.

X-ray diffraction (XRD) patterns and Li^+ conductivities at 30 °C and the corresponding activation energies are shown in Figure 2 for a series of LPS-*x*-THF/*o*-xylene, compared with those of LPS-*x*-THF. Li^+ conductivities of the samples were acquired by an alternating current (AC) method using Li^+ blocking Ti/SE/Ti symmetric cells. The XRD patterns of LPS-*x*-THF/*o*-xylene (Figure 2 a) correspond well with β-Li_3PS_4 without noticeable impurities.[13] It is noted that decreased crystallinity, reflected by peak broadening and lowered intensities, is observed as the Li deficiency increases (or the amount of added elemental sulfur increases). As *x* in LPS-*x*-THF/*o*-xylene increases up to 0.20, Li^+ conductivity is maintained at approximately 0.2 mS cm^{-1} (Figure 2 b). At $x > 0.20$, Li^+ conductivity gradually decreases to 0.062 mS cm^{-1}. In stark contrast, $Li_{2.85}PS_4$ obtained by using a single solvent (LPS-0.15-THF) shows a distinct unknown impurity phase in the XRD pattern (Figure 2 a) and correspondingly five-fold lower Li^+ conductivity (0.035 mS cm^{-1}), compared with 0.2 mS cm^{-1} for $Li_{2.85}PS_4$, was obtained (Figure 2 b). In short, the results of particle size analysis, XRD, and Li^+ conductivity strongly indicate a beneficial role of the cosolvent *o*-xylene for facilitating the homogeneous liquid-phase reaction of Li-deficient $Li_{3-x}PS_4$.

Local structures of thiophosphate polyhedra from wet-chemically derived $Li_{3-x}PS_4$ were investigated by Raman and X-ray photoelectron spectroscopy (XPS) measurements (Figure 3). Raman spectra are normalized to the main peak of Li_3PS_4 (PS_4^{3-}, 423 cm^{-1}, denoted "^"). The Raman spectrum of LPS-0.15-THF/*o*-xylene is compared with those of LPS-0.15-THF and LPS-0.00-THF/*o*-xylene in Figure 3 a. The strong signature of PS_4^{3-} for β-Li_3PS_4 is seen in all samples. Notably, only LPS-0.15-THF/*o*-xylene shows a shoulder at approximately 405 cm^{-1}, which corresponds to $P_2S_7^{4-}$.[5b,23] Considering charge compensation by increasing the Li deficiency from Li_3PS_4 ($Li_{3-x}PS_4$), PS_4^{3-} could be oxidized to $P_2S_7^{4-}$ analogs (denoted as "$P_2S_{7+n}^{4-n}$") with a bridging sulfur. The suggested model illustrated in Figure 3 a is consistent with previous reports: theoretical calculations for polymerization of Li_3PS_4,[24] electrochemically active sulfur-rich phosphorus sulfide,[25] and anion redox in Li_3PS_4.[26] Notably, the signature of $P_2S_{7+n}^{4-}$ is not observed in the $Li_{2.85}PS_4$ obtained by using the single solvent (LPS-0.15-THF). This implies that elemental sulfur in the single-solvent

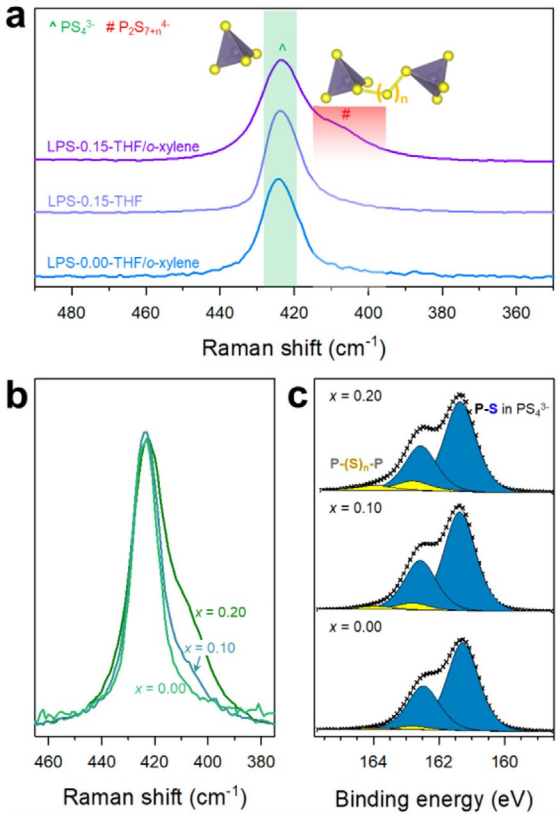

Figure 3. Raman spectra of (a) LPS-*x*-THF/*o*-xylene compared with LPS-*x*-THF and (b) as a function of *x*. (c) S 2p XPS spectra (thin "X") and the fitted results (solid lines) for LPS-*x*-THF/*o*-xylene with $x = 0.00$, 0.10, and 0.20.

case hardly participates in the reaction, which should lead to inhomogeneity of the product. This is in line with the evolution of impurities and the correspondingly much lower Li^+ conductivity of LPS-0.15-THF (Figure 2). Moreover, Raman and XPS spectra of a series of $Li_{3-x}PS_4$ ($x=0.00$, 0.10, and 0.20) derived by using dual solvents show increasing intensity for the shoulder related to $P_2S_{7+n}^{4-}$ as x is increased (Figure 3b,c).[4h,5b] The P-$[S]_n$-P signals (162.7 eV) in the XPS spectra show a gradual increase in bridging sulfur. The fraction of P-$[S]_n$-P (162.7 eV) calculated from the deconvoluted peaks increases from 3.0% at $x=0.00$ to 9.1% at $x=0.20$.

It is noted that, although previously reported $Li_{9.6}P_3S_{12}$ and $Li_3PS_{3.83}$ showed different crystal structures from Li_3PS_4,[4c,12] the wet-chemically derived $Li_{3-x}PS_4$ in this work retained the structure of β-Li_3PS_4. The structural complexity of binary Li_2S-P_2S_5 glass-ceramics arises from an appreciable amount of coexisting glassy phases, which are not accessible by conventional XRD methods but contribute significantly to the overall Li^+ conductivity.[5b] The complementary analysis from XRD, Raman, and XPS measurements, and the lowered crystallinity upon increasing the Li deficiency in $Li_{3-x}PS_4$ could indicate an increased fraction of amorphous phase enriched with $P_2S_{7+n}^{4-}$.

The electrochemical stability of wet-chemically derived $Li_{3-x}PS_4$ ($x=0.00$, 0.10) by using dual solvents was assessed by cyclic voltammetry experiments between 1.5 and 5.0 V (vs. Li/Li^+) at a scan rate of 20 mV s^{-1} (Figure S2). Compared with the stoichiometric $Li_{3.00}PS_3$, Li-deficient $Li_{2.90}PS_4$ exhibited slightly lower and higher current densities in the high and low voltage regions, respectively. This result likely indicates slightly better oxidation stability of $Li_{2.90}PS_4$ than $Li_{3.00}PS_4$, which could be associated with the amount of $P_2S_{7+n}^{4-}$ present.

Finally, $LiCoO_2$/Li-In all-solid-state cells employing wet-chemically tuned $Li_{3-x}PS_4$ (LPS-*x*-THF/*o*-xylene or LPS-*x*-THF) were cycled between 3.0 and 4.3 V (vs. Li/Li^+) at 30 °C or 70 °C. Highly conductive $Li_6PS_5[Cl,Br]$ (8.3 mS cm^{-1} at 30 °C) was employed for the SE layers, which allows us to precisely evaluate cathode performances with varied SEs. Figure 4a compares the first-cycle charge/discharge voltage profiles of $LiCoO_2$ using LPS-0.15-THF/*o*-xylene with those of $LiCoO_2$ using LPS-0.15-THF at 0.1 C and 30 °C. $LiCoO_2$ using LPS-0.15-THF/*o*-xylene shows a discharge capacity of 131 mA h g^{-1}, significantly outperforming $LiCoO_2$ using LPS-0.15-THF (108 mA h g^{-1}). Consistently, the discharge capacities at different C rates (Figure 4b) are much higher for $LiCoO_2$ with $Li_{2.85}PS_4$ using dual solvents than with $Li_{2.85}PS_4$ using a single solvent. These results are also in agreement with a much larger semicircle for $LiCoO_2$ with LPS-0.15-THF than with LPS-0.15-THF/*o*-xylene in the Nyquist plots (Figure S3). The much lower Li^+ conductivity (0.035 mS cm^{-1} vs. 0.2 mS cm^{-1}, Figure 2b) and/or the existence of larger particles (≥30 μm, Figure 1d) for LPS-0.15-THF than for LPS-0.15-THF/*o*-xylene could be responsible for the resulting electrochemical performance (Figure 4a,b). Furthermore, $LiCoO_2$ with LPS-0.10-THF/*o*-xylene was cycled between 3.0–4.3 V (vs. Li/Li^+) at 0.4 C and 70 °C (Figure 4c). The temperature of 70 °C is not available for the operation of conventional lithium-ion batteries using organic liquid electrolytes.[18a] At 70 °C, the ASLB employing $LiCoO_2$ with LPS-0.10-THF/*o*-xylene shows an initial discharge

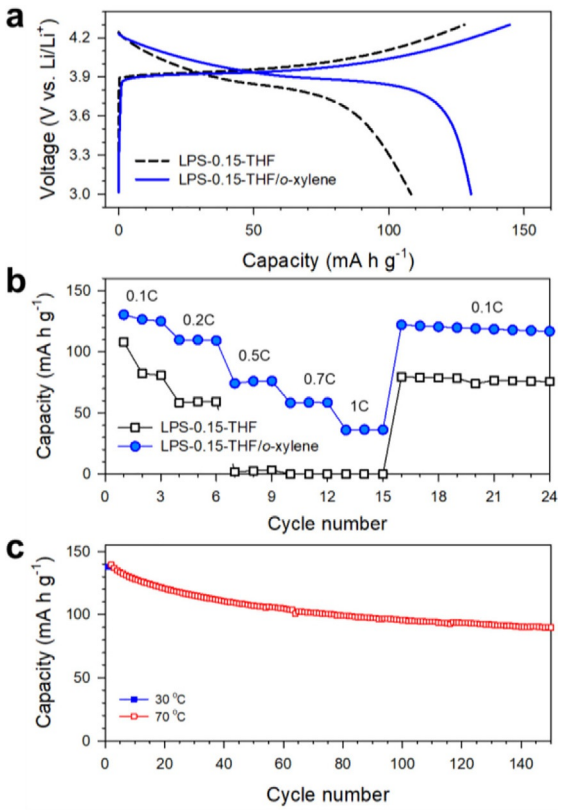

Figure 4. Electrochemical performance of $LiCoO_2$ electrodes employing wet-chemically tuned LPS-*x*-THF/*o*-xylene in $LiCoO_2$/Li-In half cells. (a) First-cycle charge/discharge voltage profiles of $LiCoO_2$ employing LPS-0.15-THF/*o*-xylene and LPS-0.15-THF at 0.1 C and 30 °C and (b) their corresponding rate capabilities. (c) Cycling performance of $LiCoO_2$ employing LPS-0.10-THF/*o*-xylene cycled between 3.0–4.3 V (vs. Li/Li^+) at 0.1 C and 30 °C for the first cycle and subsequently at 0.4 C and 70 °C.

capacity of 138 mA h g^{-1} and demonstrates remarkable cycling retention of 64.4% after 150 cycles, showing stable operation under harsh conditions. Similar cycling performance of $LiCoO_2$ was also obtained with LPS-0.15-THF/*o*-xylene (Figure S5). Finally, a rocking-chair $LiCoO_2$/graphite ASLB employing LPS-0.15-THF/*o*-xylene was tested in the voltage range of 2.5–4.2 V at 0.3 C (0.53 mA cm^{-2}) at 70 °C (Figure S6), showing a reversible capacity of 120 mA h g^{-1} and cycle retention of 83.7% after 30 cycles.

Unfortunately, only marginal improvement in electrochemical performance was achieved by fine tuning of $Li_{3-x}PS_4$ by the wet-chemical method in our model system ($LiCoO_2$ using $Li_{2.90}PS_4$ (138 mA h g^{-1} at 0.1 C and 30 °C), compared with using $Li_{3.00}PS_4$ (129 mA h g^{-1}, Figure S4). However, our results suggest a wider strategy for designing new superionic conductors, which may be able to provide improved performance in other systems.

In summary, the wet-chemical tuning of $Li_{3-x}PS_4$ ($0 \le x \le 0.3$) was demonstrated by the use of the cosolvent *o*-xylene, which is miscible with THF and dissolves elemental sulfur. $Li_{3-x}PS_4$ ($0 \le x \le 0.2$) derived by using the dual solvents showed higher Li^+ conductivity of approximately 0.2 mS cm^{-1} at 30 °C without impurities and a narrower particle size distribution, compared with that derived by using a conventional single-solvent ap-

proach. Complementary analyses by XRD, Raman, and XPS measurements suggest the evolution of $P_2S_{7+n}^{4-}$ in the amorphous phase upon decreasing the amount of Li in $Li_{3-x}PS_4$ ($0 \leq x \leq 0.2$). $LiCoO_2$/Li-In ASLBs employing $Li_{2.85}PS_4$ wet-chemically derived by using dual solvents significantly outperformed cells made with those using the conventional single solvent. Moreover, the remarkable reversibility of $LiCoO_2$ with $Li_{2.90}PS_4$ in ASLBs at 70 °C was highlighted. It is emphasized that our work is the first attempt of composition tuning for sulfide SEs by a wet-chemical route. We believe that our proof-of-concept provides new insight for designing sulfide SEs and engineering wet-chemical synthetic routes and is relevant to the development of practical all-solid-state technologies.

Experimental Section

Preparation of materials

$Li_{3-x}PS_4$ ($0 \leq x \leq 0.3$) were obtained through wet-chemical routes using THF or THF/*o*-xylene. Residual water in THF (99.9%, anhydrous, Sigma–Aldrich) and *o*-xylene (97%, anhydrous, Sigma–Aldrich) was removed by treating with molecular sieves prior to use. Stoichiometric mixtures of Li_2S (99.9%, Alfa-Aesar), P_2S_5 (99.9%, Sigma–Aldrich), and sulfur (99.5%, Alfa-Aesar) solution (20 mg mL^{-1} in *o*-xylene) were added in THF and stirred at 30 °C for 9 h, followed by drying at 80 °C for 2 h and subsequent heat-treatment at 150 °C for 1 h under vacuum. Detailed information for the targeted stoichiometry is shown in Table S1. Argyrodite Li_6PS_5[Cl,Br] for separating the SE layer in $LiCoO_2$/Li-In cells was prepared by a mechanochemical method. Stoichiometric mixtures (5 g) of Li_2S, P_2S_5, and LiCl (99.99%, Alfa-Aesar), and LiBr (99.99%, Alfa-Aesar) were milled by using a planetary ball mill (Pulverisette 7PL, Fritsch GmbH) with a zirconia vial (80 mL) with 15 zirconia balls (10 mm in diameter) and heat-treated in a fused silica ampoule sealed under vacuum at 550 °C for 10 h. $LiCoO_2$ coated with 0.3 wt% $LiNbO_3$ was used.[4e]

Materials characterization

The morphology and particle size distribution were measured by using FESEM (S-4800, Hitachi) and particle size analyzer (S3500, Microtrac). The XRD measurements were conducted with a MiniFlex600 (CuK_α radiation is 1.54056 Å) at 40 kV and 40 mA. To avoid air exposure, SE powder samples were sealed by using a Be window and mounted. Raman spectra were collected by using an NRS-3100 (JASCO) with a vis-NIR 532 nm laser. XPS results were acquired by using a K-Alpha+ (Thermo Fisher) with a monochromatic AlK_α source (1486.6 eV) at 72 W, 12 kV, and 6 mA.

Electrochemical characterization

AC impedance data were measured by using a VSP-300 (Biologics) with an amplitude of 14.1 mV in the range of 1.5 MHz to 10 mHz. The $LiCoO_2$ cathodes with wet-chemically tuned $Li_{3-x}PS_4$ were prepared by manual mixing. The weight ratio of $LiCoO_2$/$Li_{3-x}PS_4$/super C65 was 70:30:3. $Li_{0.5}In$ (nominal composition) electrodes were prepared by mixing In (99%, Sigma–Aldrich), Li powder (FMC Lithium Corp.), and SEs, following a previously reported procedure.[2] To fabricate $LiCoO_2$/Li-In cells, argyrodite Li_6PS_5[Cl,Br] powders (150 mg) were pelletized by cold-pressing to form an SE layer. The as-prepared electrodes of $LiCoO_2$ and Li-In were spread on each side of the SE layer. The mass loadings of the cathode and anode were 20 mg and 100 mg, respectively. Lastly, the tri-layers were pelletized at 370 MPa and room temperature. For $LiCoO_2$/graphite all-solid-state full cells, the mass loadings for $LiCoO_2$ electrode, LPS-0.15-THF/*o*-xylene as the SE layer, and graphite electrode were 15.1, 113, and 11.3 mg cm^{-2}. The weight ratios of active material/LPS-0.15-THF/*o*-xylene were 70:30 for the $LiCoO_2$ electrode and 60:40 for the graphite electrode.

The pelletizers and mold were Ti and polyaryletheretherketone (PEEK) mold (13 mm in diameter). The whole assembling procedure was performed in an Ar-filled glovebox. The all-solid-state cells were tested under an external pressure of 70 MPa. For the cyclic voltammetry experiments, Ti/$Li_{3-x}PS_4$/Li-In cells were used.

Acknowledgements

This was supported by the Materials and Components Technology Development Program of MOTIE/KEIT (grant no. 10076731) and by the research fund of Hanyang University (grant no. HY-2018).

Conflict of interest

The authors declare no conflict of interest.

Keywords: batteries · liquid-phase synthesis · lithium · solid electrolytes · solvent effects

[1] a) J. Janek, W. G. Zeier, *Nat. Energy* **2016**, *1*, 16141; b) X. Han, Y. Gong, K. Fu, X. He, G. T. Hitz, J. Dai, A. Pearse, B. Liu, H. Wang, G. Rubloff, Y. Mo, V. Thangadurai, E. D. Wachsman, L. Hu, *Nat. Mater.* **2017**, *16*, 572; c) A. Manthiram, X. Yu, S. Wang, *Nat. Rev. Mater.* **2017**, *2*, 16103; d) Y. Yan, R.-S. Kühnel, A. Remhof, L. Duchêne, E. C. Reyes, D. Rentsch, Z. Łodziana, C. Battaglia, *Adv. Energy Mater.* **2017**, *7*, 1700294; e) K. H. Park, Q. Bai, D. H. Kim, D. Y. Oh, Y. Zhu, Y. Mo, Y. S. Jung, *Adv. Energy Mater.* **2018**, *8*, 1800035.

[2] a) Y. J. Nam, D. Y. Oh, S. H. Jung, Y. S. Jung, *J. Power Sources* **2018**, *375*, 93 – 101; b) D. Y. Oh, Y. J. Nam, K. H. Park, S. H. Jung, K. T. Kim, A. R. Ha, Y. S. Jung, *Adv. Energy Mater.* **2019**, *9*, 1802927.

[3] a) A. Sakuda, A. Hayashi, M. Tatsumisago, *Sci. Rep.* **2013**, *3*, 2261; b) Y. Liu, Q. Sun, D. Wang, K. Adair, J. Liang, X. Sun, *J. Power Sources* **2018**, *393*, 193 – 203.

[4] a) T. A. Yersak, T. Evans, J. M. Whiteley, S.-B. Son, B. Francisco, K. H. Oh, S.-H. Lee, *J. Electrochem. Soc.* **2014**, *161*, A663 – A667; b) D. Y. Oh, Y. J. Nam, K. H. Park, S. H. Jung, S.-J. Cho, Y. K. Kim, Y.-G. Lee, S.-Y. Lee, Y. S. Jung, *Adv. Energy Mater.* **2015**, *5*, 1500865; c) Y. Kato, S. Hori, T. Saito, K. Suzuki, M. Hirayama, A. Mitsui, M. Yonemura, H. Iba, R. Kanno, *Nat. Energy* **2016**, *1*, 16030; d) X. Yao, D. Liu, C. Wang, P. Long, G. Peng, Y.-S. Hu, H. Li, L. Chen, X. Xu, *Nano Lett.* **2016**, *16*, 7148 – 7154; e) D. H. Kim, D. Y. Oh, K. H. Park, Y. E. Choi, Y. J. Nam, H. A. Lee, S.-M. Lee, Y. S. Jung, *Nano Lett.* **2017**, *17*, 3013 – 3020; f) R. P. Rao, H. Chen, L. L. Wong, S. Adams, *J. Mater. Chem. A* **2017**, *5*, 3377 – 3388; g) F. Han, J. Yue, X. Zhu, C. Wang, *Adv. Energy Mater.* **2018**, *8*, 1703644; h) S. H. Jung, K. Oh, Y. J. Nam, D. Y. Oh, P. Brüner, K. Kang, Y. S. Jung, *Chem. Mater.* **2018**, *30*, 8190 – 8200.

[5] a) A. Hayashi, S. Hama, H. Morimoto, M. Tatsumisago, T. Minami, *J. Am. Ceram. Soc.* **2001**, *84*, 477 – 479; b) C. Dietrich, D. A. Weber, S. J. Sedlmaier, S. Indris, S. P. Culver, D. Walter, J. Janek, W. G. Zeier, *J. Mater. Chem. A* **2017**, *5*, 18111 – 18119.

[6] H.-J. Deiseroth, S.-T. Kong, H. Eckert, J. Vannahme, C. Reiner, T. Zaiß, M. Schlosser, *Angew. Chem. Int. Ed.* **2008**, *47*, 755 – 758; *Angew. Chem.* **2008**, *120*, 767 – 770.

[7] a) N. Kamaya, K. Homma, Y. Yamakawa, M. Hirayama, R. Kanno, M. Yonemura, T. Kamiyama, Y. Kato, S. Hama, K. Kawamoto, A. Mitsui, *Nat.*

Mater. **2011**, *10*, 682 – 686; b) P. Bron, S. Johansson, K. Zick, J. R. Schmedt auf der Günne, S. Dehnen, B. Roling, *J. Am. Chem. Soc.* **2013**, *135*, 15694 – 15697.

[8] A. Hayashi, K. Noi, A. Sakuda, M. Tatsumisago, *Nat. Commun.* **2012**, *3*, 856.

[9] A. Banerjee, K. H. Park, J. W. Heo, Y. J. Nam, C. K. Moon, S. M. Oh, S.-T. Hong, Y. S. Jung, *Angew. Chem. Int. Ed.* **2016**, *55*, 9634 – 9638; *Angew. Chem.* **2016**, *128*, 9786 – 9790.

[10] a) M. Duchardt, U. Ruschewitz, S. Adams, S. Dehnen, B. Roling, *Angew. Chem. Int. Ed.* **2018**, *57*, 1351 – 1355; *Angew. Chem.* **2018**, *130*, 1365 – 1369; b) J. W. Heo, A. Banerjee, K. H. Park, Y. S. Jung, S.-T. Hong, *Adv. Energy Mater.* **2018**, *8*, 1702716; c) Z. Zhang, E. Ramos, F. Lalère, A. Assoud, K. Kaup, P. Hartman, L. F. Nazar, *Energy Environ. Sci.* **2018**, *11*, 87 – 93.

[11] a) H. Muramatsu, A. Hayashi, T. Ohtomo, S. Hama, M. Tatsumisago, *Solid State Ionics* **2011**, *182*, 116 – 119; b) G. Sahu, Z. Lin, J. Li, Z. Liu, N. Dudney, C. Liang, *Energy Environ. Sci.* **2014**, *7*, 1053 – 1058.

[12] M. Park, H.-G. Jung, W. D. Jung, S. Y. Cho, B.-N. Yun, Y. S. Lee, S. Choi, J. Ahn, J. Lim, J. Y. Sung, Y.-J. Jang, J.-P. Ahn, J.-H. Lee, H. Kim, *ACS Energy Lett.* **2017**, *2*, 1740 – 1745.

[13] Z. Liu, W. Fu, E. A. Payzant, X. Yu, Z. Wu, N. J. Dudney, J. Kiggans, K. Hong, A. J. Rondinone, C. Liang, *J. Am. Chem. Soc.* **2013**, *135*, 975 – 978.

[14] S. Yubuchi, S. Teragawa, K. Aso, K. Tadanaga, A. Hayashi, M. Tatsumisago, *J. Power Sources* **2015**, *293*, 941 – 945.

[15] a) K. H. Park, D. Y. Oh, Y. E. Choi, Y. J. Nam, L. Han, J.-Y. Kim, H. Xin, F. Lin, S. M. Oh, Y. S. Jung, *Adv. Mater.* **2016**, *28*, 1874 – 1883; b) Y. E. Choi, K. H. Park, D. H. Kim, D. Y. Oh, H. R. Kwak, Y.-G. Lee, Y. S. Jung, *ChemSusChem* **2017**, *10*, 2605 – 2611.

[16] E. Rangasamy, Z. Liu, M. Gobet, K. Pilar, G. Sahu, W. Zhou, H. Wu, S. Greenbaum, C. Liang, *J. Am. Chem. Soc.* **2015**, *137*, 1384 – 1387.

[17] D. A. Ziolkowska, W. Arnold, T. Druffel, M. Sunkara, H. Wang, *ACS Appl. Mater. Interfaces* **2019**, *11*, 6015 – 6021.

[18] a) D. Y. Oh, D. H. Kim, S. H. Jung, J.-G. Han, N.-S. Choi, Y. S. Jung, *J. Mater. Chem. A* **2017**, *5*, 20771 – 20779; b) S. Choi, S. Lee, J. Park, W. T. Nichols, D. Shin, *Appl. Surf. Sci.* **2018**, *444*, 10 – 14.

[19] D. H. Kim, H. A. Lee, Y. B. Song, J. W. Park, S.-M. Lee, Y. S. Jung, *J. Power Sources* **2019**, *426*, 143 – 150.

[20] H.-D. Lim, X. Yue, X. Xing, V. Petrova, M. Gonzalez, H. Liu, P. Liu, *J. Mater. Chem. A* **2018**, *6*, 7370 – 7374.

[21] Q. Pang, X. Liang, A. Shyamsunder, L. F. Nazar, *Joule* **2017**, *1*, 871 – 886.

[22] S. Yubuchi, M. Uematsu, C. Hotehama, A. Sakuda, A. Hayashi, M. Tatsumisago, *J. Mater. Chem. A* **2019**, *7*, 558 – 566.

[23] Y. Wang, D. Lu, M. Bowden, P. Z. El Khoury, K. S. Han, Z. D. Deng, J. Xiao, J.-G. Zhang, J. Liu, *Chem. Mater.* **2018**, *30*, 990 – 997.

[24] M. Sumita, Y. Tanaka, T. Ohno, *J. Phys. Chem. C* **2017**, *121*, 9698 – 9704.

[25] X. Li, J. Liang, Y. Lu, Z. Hou, Q. Cheng, Y. Zhu, Y. Qian, *Angew. Chem. Int. Ed.* **2017**, *56*, 2937 – 2941; *Angew. Chem.* **2017**, *129*, 2983 – 2987.

[26] T. Hakari, M. Deguchi, K. Mitsuhara, T. Ohta, K. Saito, Y. Orikasa, Y. Uchimoto, Y. Kowada, A. Hayashi, M. Tatsumisago, *Chem. Mater.* **2017**, *29*, 4768 – 4774.

Manuscript received: July 8, 2019
Revised manuscript received: September 11, 2019
Accepted manuscript online: September 17, 2019
Version of record online: October 22, 2019